

1 **Remote sensing chlorophyll *a* mapping of optically complex waters**  
2 **(rias Baixas, NW Spain): Application of a regionally specific**  
3 **chlorophyll *a* algorithm for MERIS full resolution data during an**  
4 **upwelling cycle**

5  
6 Evangelos Spyrakos <sup>a</sup>, Luis González Vilas <sup>a</sup>, Jesus M. Torres Palenzuela <sup>a,\*</sup>, Eric  
7 Desmond Barton <sup>b</sup>

8  
9 <sup>a</sup>Remote Sensing and GIS Laboratory. Department of Applied Physics. Sciences  
10 Faculty. University of Vigo. Campus Lagoas Marcosende. 36310. Vigo. Spain

11 <sup>b</sup>Instituto de Investigaciones Marinas, C/Eduardo Cabello, 6, E-36208, Vigo, Spain

12  
13  
14  
15  
16  
17  
18  
19  
20 \* Corresponding author: Tel. +34 986 812 631. Fax: +34 986 812 556. E-mail address:

21 [jesu@uvigo.es](mailto:jesu@uvigo.es) (J. M. Torres-Palenzuela).

22

23 **Abstract**

24 This study takes advantage of a regionally specific algorithm and the characteristics of  
25 Medium Resolution Imaging Spectrometer (MERIS) in order to deliver more accurate,  
26 detailed chlorophyll *a* (chl<sub>a</sub>) maps of optically complex coastal waters during an  
27 upwelling cycle. MERIS full resolution chl<sub>a</sub> concentrations and *in situ* data were  
28 obtained in three Galician *rias* (NW Spain) and the adjacent shelf, an area of extensive  
29 mussel cultures that experiences frequent harmful algal events. Regionally focused  
30 algorithms (NNRB) for the retrieval of chl<sub>a</sub> in the Galician *rias* optically complex  
31 waters were tested in comparison to sea-truth data and the one that showed the best  
32 performance was applied in a series of six MERIS (FR) images during a summer  
33 upwelling cycle to test its performance. The best performance parameters were given  
34 for the NN trained with high-quality data using the most abundant cluster found in the  
35 *rias* after the application of fuzzy c-mean clustering techniques (FCM). July 2008 was  
36 characterized by three periods of different meteorological and oceanographic states. The  
37 main changes in chl<sub>a</sub> concentration and distribution were clearly captured in the images.  
38 After a period of a strong upwelling favourable winds a high biomass algal event was  
39 recorded in an area of low SST. However, MERIS missed the high chlorophyll  
40 upwelled water that was detected below surface in the *ria de Vigo* by the chl<sub>a</sub> profiles,  
41 proving the necessity of *in situ* observations. Relatively high biomass "patches" were  
42 mapped in detail inside the *rias*. There was a significant variation in the timing and the  
43 extent of the maximum chl<sub>a</sub> areas. The maps confirmed that the spatial structure of the  
44 phytoplankton distribution in the study area can be complex. Surface currents and winds  
45 off the *rias Baixas* affected the distribution of chl<sub>a</sub> in the *rias Baixas*. This study  
46 showed that a regionally specific algorithm for an ocean colour sensor with the  
47 characteristics of MERIS in combination with *in situ* data can be of great help in chl<sub>a</sub>

48 monitoring, detection and study of high biomass algal events in an area affected by  
49 coastal upwelling such as the *rias Baixas*.

50

51 Keywords: Chlorophyll *a*, MERIS, algorithms, upwelling, Galician *rias*

52

### 53 **Highlights**

54 > We apply regionally specific chlorophyll *a* algorithms from MERIS data. >We study  
55 chlorophyll *a* distribution coupled with *in-situ* data during upwelling. >We provide  
56 more accurate chlorophyll *a* maps of optically complex coastal waters. >Images  
57 captured the main changes in chlorophyll *a* concentration and distribution. >

58

59

60

61

62

63

64

65

66

67

## 69 **1. Introduction**

70 Among ocean-colour derived data, chlorophyll *a* (*chl<sub>a</sub>*) concentration is the most used  
71 product since it provides a good estimation of phytoplankton biomass and is common to  
72 almost all taxonomic groups (Jeffrey et al., 1997). The phytoplankton community  
73 responds rapidly to environmental changes (EC, 2000), which can cause visible changes  
74 in chlorophyll in the surface waters.

75 The estimation of *chl<sub>a</sub>* concentration in the oceans from the first dedicated ocean colour  
76 scanner (CZCS) that launched in 1978 and operated until 1986 provided useful  
77 information on the global distribution of *chl<sub>a</sub>* but the quality of the data was limited  
78 (Robinson, 2004). The Sea-viewing Wide-Field-view Sensor (SeaWiFS), Moderate  
79 Resolution Imaging Spectroradiometer (MODIS) and the most recent Medium  
80 Resolution Imaging Spectrometer (MERIS) that succeeded CZCS are using more and  
81 narrower spectral bands and finer spatial resolution. MERIS provides data with a 300 m  
82 on-ground resolution in nadir (Full Resolution) and has a spectral resolution of fifteen  
83 bands from visible to near infra red, supporting one of the mission objectives for  
84 delicate coastal zone monitoring (Doerffer et al., 1999).

85 Traditionally, *chl<sub>a</sub>* is estimated using empirical algorithms based on the ratio between  
86 the radiance of blue and green light reflected by the sea. For the retrieval of *chl<sub>a</sub>* from  
87 ocean colour sensors various empirical spectral-ratio algorithms (Evans and Gordons,  
88 1994; Muller-Karger et al., 1990; Aiken et al., 1995; McClain et al., 2004; O' Reilly et  
89 al., 2000; Brown et al., 2008) and semi-analytical models (Gardner and Steward, 1985;  
90 Gardner et al., 1999) were developed. In typical case II waters, where high  
91 concentrations of water constituents (CDOM, detritus) absorb strongly in the blue

92 decoupling the phytoplankton absorbance, this ratio cannot be used for an accurate  
93 retrieval of chl $a$  (Morel and Prieur 1977; Gons, 1999; Gitenlson *et al.*, 2007).

94 In the effort for more accurate retrieval of water constituents in optically complex  
95 waters, neural network (NN) techniques can play an important role, since they seem  
96 ideal for multivariate, complex and non-linear data modelling (Thiria, 1993). In the last  
97 decades the application of neural network (NN) techniques for the estimation of selected  
98 water quality parameters from ocean-colour has increased (Atkinson and Tatnall, 1997;  
99 Keiner and Yan, 1998; Dzwonkowski and Yan, 2005; Zhang *et al.*, 2003; Shahraiyni *et*  
100 *al.*, 2009). Dransfeld *et al.*, (2004) proposed that studies for development of ocean  
101 colour algorithms should be regionally specific and emphasised the role of NNs in the  
102 retrieval of water constituents especially in Case 2 waters. NN based algorithms are  
103 currently used as standard products for the estimation of chl $a$ , SPM and yellow  
104 substances by the European Space Agency (ESA) for MERIS data (Doerffer and  
105 Schiller, 2007, 2008).

106 Although remote sensing tools can be used with a relatively high precision at global  
107 scale for the calculation of chl $a$ , they are not always totally accurate in local areas  
108 (Ruddick *et al.*, 2008). Validation methods and development or expansion of chl $a$   
109 algorithms for specific areas have been widely used to test and regionalize the satellite  
110 products (e.g. Gons *et al.*, 2002; Cota *et al.*, 2004; Witter *et al.*, 2009).

111 In the Galician *rias* (NW Spain) the interest in developing an accurate estimation of  
112 chl $a$  is considerable, mainly because of the economic and social importance of the  
113 extensive culture of mussels, and the frequent occurrence of harmful algal events  
114 (GEOHAB, 2005).

115 In the present paper a neural network-based chl<sub>a</sub> algorithm previously developed for the  
116 Galician *rias* waters (within the *rias* and for coastal waters on the continental shelf)  
117 was applied for the first time in a short series of MERIS (FR) images delivered during  
118 an upwelling cycle in order to obtain maps of chl<sub>a</sub>. The performance of the neural  
119 network-based chl<sub>a</sub> algorithm is compared to *in situ* measurements and other algorithms  
120 that are routinely used for MERIS data. The temporal and spatial distribution of the chl<sub>a</sub>  
121 patterns that were captured in the MERIS images using the local adapted algorithm in  
122 relation to the meteorological and oceanographic conditions in the area are also  
123 discussed.

## 124 **2. Methods and data**

### 125 2.1 Description of the study area

126 The Galician *rias* are V-like coastal formations along the northwest part of the Iberian  
127 Peninsula (Fig. 1). The *rias Baixas* constitute the southern part of the Galician *rias*.  
128 They are formed by four large coastal embayments, from north to south: *Muros y Noya*,  
129 *Arousa*, *Pontevedra* and *Vigo*, all oriented in a SW-NE direction, and characterized by  
130 strong tides. Surface area covers approximately 600 km<sup>2</sup> and water depths range from 5-  
131 60 m. This study focuses on three *rias* (*Arousa*, *Pontevedra* and *Vigo*), each connected  
132 to the open sea through two entrances, to the north and south of the islands located at  
133 the external part of each *ria*. The *ria de Vigo* is the longest of the *rias* whereas the *ria*  
134 *de Arousa* is the widest one. *Rias* vary in width from 1-3 km in their inner part to 8-12  
135 km in their external part (Vilas et al., 2005). The main freshwater inputs in the *rias* are  
136 by rivers that located in innermost part of the *rias*.

137 In these highly primary productive upwelling estuarine systems (Fraga, 1981; Torres &  
138 Barton, 2007) transient increases of phytoplankton abundance, referred to as blooms,

139 are a frequent phenomenon occurring mainly between early spring and late fall (Fraga,  
140 1988; Varela, 1992; Figueiras & Ríos, 1993). Sporadically, some phytoplankton blooms  
141 in the Galician *rias* are perceived as harmful with direct and indirect impacts to the  
142 mussel production that constitute an important economic activity in the area. Harmful  
143 algal events in the Galician *rias* are a well documented phenomenon. Several studies  
144 since the 1950s referred to the harmful algal events and in general to phytoplankton  
145 ecology on the Galician *rias* particularizing favourable conditions to the development of  
146 HABs, their origin, dynamic, distribution and toxicity levels (Margalef, 1956; Tillstone  
147 et al., 1994; Figueiras et al., 1994; GEOHAB, 2005), seasonal taxonomic and chemical  
148 composition of phytoplankton and picophytoplankton, "patchiness" (Figueiras & Niell,  
149 1987; Nogueira et al., 1997; Tillstone et al., 2003). Despite the fact that an ocean colour  
150 sensor with the characteristics of MERIS is considered adequate for *chl a* monitoring  
151 and detection of HABs in coastal areas, to our knowledge the number of studies using  
152 MERIS data in the Galician *rias* is limited those of Torres Palenzuela et al. (2005a;  
153 2005b) and González Vilas et al. (2011). The latter authors developed a *chl a* algorithm  
154 based on NNs and classification techniques from MERIS full resolution data for *rias*  
155 *Baixas* coastal waters.

## 156 2.2 Sampling regime

157 Two samplings were conducted in 2008 in the *ria de Vigo*. Twelve fixed stations were  
158 visited on cloud-free days (July 9 and 22). The sampling transect extended from the  
159 open sea towards to the inner part of the *ria*. Satellite data from MERIS (FR) were  
160 available for the same days. The depth of the stations ranged from 5 m inside the *ria* to  
161 100 m outside. Triplicate water samples from surface to 3 meters were collected at each  
162 station from a sampler (3524 cm<sup>3</sup>) for the determination of HPLC pigments and SPM.

### 163 2.3 *In situ* measurements

164 *In situ* chl $a$  fluorescence profile was monitored by a Turner designs CYCLOPS-7  
165 submersible fluorometer. Profiles of water temperature were provided by a portable  
166 meter (HI 9829, Hanna instruments). The depth of the euphotic zone was established  
167 with a Secchi disk. For the High Performance Liquid Chromatography (HPLC) chl $a$   
168 determination, water samples (100-200mL) were filtered through 9mm diameter  
169 Whatman GF/F filters and stored at -80°C for two weeks, and 95% methanol was used  
170 as extraction solvent for the pigments. In this study only chl $a$  concentration data are  
171 presented, calculated as the sum of chlorophyllide  $a$ , chlorophyll  $a$  epimer, chlorophyll  
172  $a$  allomer and divinyl chlorophyll  $a$ . An HPLC method using a reversed phase C $_8$  was  
173 applied for the separation of the pigments. Details of pigment extraction and separation  
174 are provided in Zapata *et al.* (2000).

175 Suspended particulate material (SPM) was evaluated in terms of SPM concentration and  
176 percent weight of organic material (%OM). Pre-combusted (450 °C for 24 h), pre-  
177 washed in 500 mL of MilliQ, 47mm Whatman GF/F filters were used. These filters  
178 were then dried at 65 °C to a constant weight. Particles were collected by filtering a  
179 standard volume (1000mL) of seawater samples and then rinsed with 50mL MilliQ in  
180 order to remove salts and dissolved organic material. For the determination of SPM the  
181 filters were dried at 65°C till no weight changes were observed. The filters were then re-  
182 combusted at 450 °C for 5 h in order to obtain the inorganic suspended material (ISM).  
183 The percent weight of organic material (%OM) was determined by subtracting the ISM  
184 from the SPM. All the filters were weighted on a Precisa 262 SMA-FR microbalance  
185 ( $10^{-5}$  g precision).

### 186 2.4 Oceanographic and meteorological data



187 Oceanographic and meteorological data off the *rias Baixas* were provided by the  
188 Spanish Port System ([www.puertos.es](http://www.puertos.es)). More specifically, wind speed (W) and  
189 direction, current data and water temperature were observed at a Seawatch buoy station  
190 located off Cape Silleiro (42° 7.8'N, 9° 23.4'W). This meteorological station was  
191 selected as fairly representative of the study area (Herrera et al., 2005). Daily upwelling  
192 index ( $I_w$ ) was estimated from wind by Bakun's (1973) method:

$$193 \quad I_w = -\tau_y / (\rho_w \cdot f) = -1000 \cdot \rho_a \cdot C_D \cdot W \cdot W_y / (\rho_w \cdot f) \quad \text{m}^3 / (\text{s} \cdot \text{km})$$

194 where  $\rho_a$  is the density of air (1.2 kg·m<sup>-3</sup> at 15°C),  $C_D$  is an empirical dimensionless drag  
195 coefficient (1.4·10<sup>-3</sup> according to Hidy, 1972),  $f$  is the Coriolis parameter (9.9·10<sup>-5</sup> s<sup>-1</sup> at  
196 42° latitude),  $\rho_w$  is the density of seawater (1025 kg·m<sup>-3</sup>), and  $W$  and  $W_y$  are the average  
197 daily module and northerly component of the wind.

198 Moderate Resolution Imaging Spectroradiometer (MODIS-Aqua) sea surface  
199 temperature (SST) daily level 2 data for July 2008 were downloaded from the website  
200 of the National Aeronautics and Space Administration Goddard Space Flight Center  
201 (NASA-GSFC) (<http://oceancolor.gsfc.nasa.gov/>). The 1 × 1 km resolution MODIS data  
202 were processed using MATLAB software to derive projected SST maps of the study  
203 area. The study area for the SST maps was expanded to 42-43° N and 9.3-8.3° W. The  
204 MODIS imagery contains 6 images for the dates that MERIS data were available.

## 205 2.5 MERIS data and MERIS chl $a$ algorithms for Case 2 waters

### 206 2.5.1 MERIS case II Regional Processor (C2R)

207 MERIS Case-2-Regional Processor (C2R) (Doerffer & Schiller, 2007, 2008) is the  
208 algorithm for chl $a$  that is currently used as a standard product by the European Space  
209 Agency (ESA) for Case 2 waters. The MERIS C2R processor takes advantage of the

210 combined NN technique to derive the optical properties of the water (absorption of  
211 pigments, yellow substance and scattering of all particles). It includes an atmospheric  
212 correction. An inverse NN is used to emulate the inverse model and a forward NN to  
213 emulate the forward model and to test if the measured spectrum is within the scope of  
214 the training set. MERIS reflectances of eight bands in the visible spectra, information  
215 about geometry and biooptical data of the water constituents are trained in the NNs. The  
216 bio-optical model used for the simulations is based on a large data set collected mainly  
217 in European waters. Among the final outputs of the algorithm is the absorption  
218 coefficient of phytoplankton pigment ( $a_{\text{pigment}}$ ). Final concentration of *chl a* is calculated  
219 according to the empirical relationship between *chl a* (*algal\_2*) and absorption  
220 coefficient ( $a_{\text{pigment}}$ ) (Doerffer & Schiller, 2005):

$$221 \quad \text{algal\_2} = 21 * a_{\text{pigment}}(443)^{1.04} \quad (1)$$

222 which permits the modification of the parameters in order to be suitable for the each  
223 study area.

#### 224 2.5.2 Regional neural network for *rias Baixas* (NNRB)

225 Developed by González Vilas et al., (2011), this set of algorithms represents feed-  
226 forward NNs trained by supervised learning using iterative back-propagation of error  
227 for the retrieval of *chl a* from MERIS FR data. These algorithms approximate sets of  
228 different classes of water-leaving radiance reflectances data, determined after the  
229 application of Fuzzy c-means clustering techniques (FCM), to a set of appropriate *chl a*  
230 concentrations. Input variables are 11 MERIS water leaving radiance reflectance and 3  
231 geometry values. It was found that MERIS data can be classified in 3 clusters (#1, #2  
232 and #3) but only one could be used for the 3 different NNs that were developed for the  
233 retrieval.

234 The method performs well in the estimation of *chl<sub>a</sub>* from MERIS (FR) data in the  
235 optically complex waters of the *rias Baixas* and detects perfectly the peaks of *chl<sub>a</sub>*.  
236 NNRB is based on *in situ* *chl<sub>a</sub>* data collected from the *rias Baixas* during a long period  
237 survey (2002-2008), covering the temporal variability of *chl<sub>a</sub>* in all the part of the *rias*.  
238 In contrast with the Schiller and Doerffer algorithm, this algorithm does not use  
239 simulated data. The result is a narrower range (0.03-7.73 mg m<sup>-3</sup>), but this is considered  
240 as sufficient for the study area.

### 241 2.5.3 Application of *chl<sub>a</sub>* algorithms to MERIS imagery

242 The MERIS satellite imagery used in this study contains 6 full-resolution level-1b  
243 images derived from the area in July 2008. MERIS overpasses were within 2 hours of  
244 the time that samples and data were collected *in situ*. Beam 4.2 (Brockmann Consult  
245 and contributors, Germany) software was used for the analysis of the imagery.

246 The BEAM-4.6's smile correction was applied to the original level-1b data. For the  
247 atmospheric correction the ocean colour data were processed with a NN-based  
248 algorithm which was developed by Doerffer and Schiller (2008). The level-2 products  
249 of the *chl<sub>a</sub>* concentrations calculated by the NNRB and the MERIS Case 2 Regional  
250 Processor (C2R) were processed with the same atmospheric correction. This NN  
251 algorithm for dedicated atmospheric correction over turbid case 2 waters is based on  
252 radiative transfer simulations. The performance test of the atmospheric correction  
253 showed increasing uncertainty with decreasing values of water leaving radiance  
254 reflectances (Doerffer & Schiller, 2008).

255 The flags for coastline, land, clouds and invalid reflectance were raised using the Beam  
256 software. Ocean colour data derived from areas significantly affected by sun glint

257 (beyond a solar zenith angle limit of  $60^\circ$ ) were characterized invalid and removed from  
258 the analysis.

259 The FCM algorithm that was proposed by González et al., (2011) was applied to the 12  
260 data in order to identify the different clusters. Classification images were then obtained  
261 for the available MERIS images using the same FCM algorithm. The pixels in these  
262 images were assigned to the cluster with the highest value in its corresponding  
263 membership function and the percentage of pixels belonging to each cluster was  
264 computed. The performance of the available algorithms was then tested and the NN  
265 with the best performance measures was applied to the MERIS leaving radiance  
266 reflectance values in order to deliver the *chl<sub>a</sub>* maps for the study area.

267 *In situ* *chl<sub>a</sub>* data points delivered from cloud-free scenes and areas that were not flagged  
268 for coastline and invalid reflectance were considered to be valid match-up data and were  
269 used for the performance testing of the *chl<sub>a</sub>* algorithms. Water-leaving radiance  
270 reflectances and *chl<sub>a</sub>* concentrations were computed as mean values of the pixel  
271 corresponding to the sampling station location and the 8 surrounding pixels. These 9  
272 pixels cover approximately  $0.8 \text{ km}^2$  of surface area and it was considered that this  
273 averaging was able to reduce MERIS instrument noise. For each sampling point, the  
274 number of pixels included in the median computation was also extracted as a quality  
275 flag, ranging from 9 (highest quality) to 1 (lowest quality). Low quality values indicate  
276 that the sampling station is located in the proximity of the coast or cloudy or foggy  
277 areas, so that the reflectance values could be affected.

278 The imagery was then remapped using the standard Mercator projection with a fixed  
279 grid of 890 by 890 pixels. Each *chl<sub>a</sub>* image ranges from  $42^\circ 04' \text{ N}$  to  $42^\circ 40' \text{ N}$  latitude  
280 and from  $8^\circ 32' \text{ W}$  to  $9^\circ 32' \text{ W}$  longitude, which covers approximately  $3.1 \times 10^3 \text{ km}^2$ .

## 281 2.6 Performance measures

282 The following statistical measurements were used to evaluate the performance of the  
283 *chl<sub>a</sub>* models. For the measured *chl<sub>a</sub>* concentration (*Chl<sub>x</sub>*) and the modelled *chl<sub>a</sub>* (*Chl $\hat{x}$* )  
284 the difference

$$285 \quad PE_i = Chl x_i - Chl \hat{x}_i \quad (2)$$

286 was noted and was used to obtain the root mean square error (RMS error) and the  
287 relative RMS error, which are defined as:

$$288 \quad RMS \ error = \sqrt{\frac{\sum_{i=1}^N PE_i^2}{N}} \quad (3)$$

$$289 \quad Rel. \ RMS \ error = \sqrt{\frac{RMSE}{\frac{1}{N} \sum_i Chl x_i}} 100 \quad (4)$$

290 In addition, the coefficient of determination ( $R^2$ ) was computed as a measurement of the  
291 correlation between the *Chl<sub>x</sub>* and the *Chl $\hat{x}$* . RMSE and relative RMSE were used in this  
292 work as measurements of absolute error (in  $mg \ m^{-3}$ ) and relative error respectively.

## 293 3. Results and discussion

### 294 3.1 *In situ* data

295 Sea-truthing ranges of HPLC *chl<sub>a</sub>*, SPM, percentage of inorganic matter and Secchi  
296 disk depth for the two samplings are given in Table 1, which also summarizes  
297 information about the available MERIS imagery. Water temperatures near surface  
298 ranged from 16.90 to 19.54 °C and from 16.58 to 18.91 °C, respectively, for the two  
299 samplings. Temperature at 10 m depth during the first sampling was between 15.33 and  
300 17.70 °C, whereas temperatures dropped to 13.50-14.47 °C at the sampling stations on  
301 July 22.

302 Water temperature decreased from the outer part towards the inner part of the *ria*.  
303 Values of Secchi disk depth between 2 to 12 m were measured in the *ria de Vigo*,  
304 generally less than half the water column depth.

305 *Chla* concentration in the surface water samples did not show a wide variation. *Chla*  
306 levels were relatively low in comparison with the temporal pattern proposed for the *rias*  
307 *Baixas* by Nogueira et al. (1997) where *chla* concentrations close to  $5 \text{ mg m}^{-3}$  are  
308 described as typical during the summer period. Mean *chla* determined by HPLC varied  
309 from 0.03 at station 12 to  $2.65 \text{ mg m}^{-3}$  in the inner part during the first sampling. On  
310 July 22 the highest *chla* concentration ( $2.72 \text{ mg m}^{-3}$ ) was recorded in the innermost *ria*  
311 station. Although the range in the surface *chla* concentration was similar in both  
312 samplings, differences were observed in the *chla* profiles. In the sampling conducted on  
313 July 9, small differences were observed in the *chla* concentration profiles in the first 10  
314 m of the water column in all stations except the three at the inner part of the *ria* where a  
315 *chla* maximum was recorded at 4 m depth (Fig. 2A). On the other hand, a vertical  
316 gradient of *chla* was detected in almost all sampling stations during the second sampling  
317 (Fig. 2B), with the highest values of *chla* (up to  $16 \text{ mg L}^{-1}$ ) found close to 10 m. The  
318 same vertical distribution pattern during the month of July in *ria de Pontevedra* is  
319 described in Varela et al. (2008) and is imputed to the presence of upwelled waters.

320 SPM concentrations varied from 1.17 to  $3.15 \text{ mg L}^{-1}$  in the *ria de Vigo* and showed  
321 decreasing values with distance from st. 1, which is located in the inner, narrow part of  
322 the *ria* and closer to the main freshwater inputs. In this part of the *ria* sediment  
323 resuspension and continental runoff is probably higher having as a result high  
324 concentrations of SPM.

325 The results of the Chl $a$  and SPM analyses of this study combined with available  
326 unpublished data from the same sampling stations using the same methodology showed  
327 that these two variables vary independently (Fig. 3, determination coefficient of linear  
328 relationship  $R^2=0.1$ ). This confirms the initial assumption that *rias Baixas* waters can  
329 be categorized as Case 2 (Morel & Prieur, 1977). This classification is not always a  
330 simple distinction of coastal and oceanic waters as Morel and Maritonema (2001)  
331 describe in a later study using a new dataset of optical properties, indicating the need for  
332 models more restricted in geographical and seasonal terms.

### 333 3.2 Classification results and comparison of MERIS chl $a$ algorithms with *in situ* data

334 Classification images, showing the cluster value for each sea pixel, were obtained for  
335 the MERIS images involved in the analysis (Fig. 4). In theory, the membership grades  
336 for each cluster would allow us to blend the chl $a$  concentration, obtained from the  
337 different neural networks developed for each cluster, into a given pixel, so that chl $a$   
338 maps with soft transitions would be created (Moore et al., 2009). In practice, the NNRB  
339 model was only developed for Cluster#1 (González Vilas et al., 2011), so that these  
340 classification images presented here were only useful for detecting the zones where  
341 Cluster#1 is the dominant cluster and therefore the areas where NNRB can be best  
342 applied to obtain more reliable results. Figure 4 shows that Cluster#1 is dominant in  
343 almost all the images in the *rias Baixas* and the adjacent area. Table 2 shows the  
344 percentage of pixels belonging to each cluster for each image over the *rias Baixas*.  
345 Cluster#1 includes the majority of the pixels in *ria de Vigo*, with more than 72% of  
346 pixels in the six images. On average, 71% and 65% of the pixels over *ria de Pontevedra*  
347 and *ria de Arousa* belong to this cluster. Cluster#2 is the predominant one in in the *ria*  
348 *de Pontevedra* and *ria de Arousa* in the image delivered on July 29. Cluster#3 is the  
349 least abundant in most of the images, with less than 3.25% of pixels in all of them.

350 However, the presence of Cluster#2 and Cluster#3 does not prevent the continuous  
351 chlorophyll mapping over large areas in the *rias*, because of the predominance of  
352 Cluster#1. The image delivered on the July 29 is more problematic (referring to the high  
353 percentage of pixels belonging to Cluster#2), although the mapping of a large part of *ria*  
354 *de Vigo* and small parts of *ria de Pontevedra* and *ria de Arousa* was possible.

355 Insofar as the two cloud-free field campaigns were designed specifically to collect  
356 samples within a time period of 2 hours from the MERIS overpasses time, 24 valid data  
357 were available to test performance of the MERIS *chl<sub>a</sub>* algorithms. The performance  
358 parameters for the match-up data of MERIS *chl<sub>a</sub>* retrieved by the C2R processor and the  
359 three NNRB algorithms (NNRB#1, NNRB#2 and NNRB#3) are shown in Table 3. The  
360 available dataset did not show a wide range of environmental variation, with *chl<sub>a</sub>*  
361 ranging from 0.03 to 2.72 mg m<sup>-3</sup>. The three NNRB algorithms outperformed the C2R  
362 showing higher R<sup>2</sup> and lower RMSE values. However, the NNRB for the Cluster#1,  
363 high quality data produced well correlated results (R<sup>2</sup>=0.70) which are much higher than  
364 the CR2 results. Bottom effects on the reflectance or the presence of macroalgae and  
365 adjacency effects might be the factors responsible for the difference in the performance  
366 parameters that was observed between NNRB#1(2) and NNRB#3. The C2R has shown  
367 good results for *chl<sub>a</sub>* retrieval in coastal areas and inland waters (Peters, 2006; Odermatt  
368 et al., 2010) but the correlation with the *in situ* data in this study was poor. The poor  
369 correlation shown by C2R may be the result of the low *chl<sub>a</sub>* concentrations that were  
370 recorded in the *ria de Vigo*. C2R is more likely to be inaccurate in low *chl<sub>a</sub>*  
371 concentrations with moderate values (>2 mg m<sup>-3</sup>) of SPM (Doerffer and Schiller, 2007).  
372 Further error may arise from sea bottom reflection especially in the innermost part of  
373 the *ria*. The good performance of NNRB#3 is not surprising considering that NNRB#3  
374 can clearly follow the cycle of chlorophyll recorded in the *rias Baixas*: concentrations



375 lower than  $1 \text{ mg m}^{-3}$  during the winter months, up to  $8 \text{ mg m}^{-3}$  during the spring and  
376 autumn maxima and close to  $5 \text{ mg m}^{-3}$  during the summer. Moreover, the NNRB  
377 algorithm is trained with MERIS and *in situ* chl<sub>a</sub> data during upwelling events.  
378 NNRB#3 seems to be robust and ideal for the *rias Baixas* coastal waters where it can be  
379 used for a more accurate mapping of chl<sub>a</sub> in order to improve the understanding of the  
380 spatial and temporal distributions.

### 381 3.3 Upwelling cycle

382 Different meteorological and oceanographic periods were identified and categorized as  
383 three different states in the area during July of 2008 (Table 4, Fig. 5). The states lasted  
384 from nine to eleven days which is typical in an upwelling cycle in the area (Nogueira et  
385 al., 1997).

#### 386 *State 1 (July 1-11)*

387 This 10 d period state comes after a strong upwelling that occurred in the area at the end  
388 of June (Fig. 5A) and it is characterized mainly by weak winds of variable direction  
389 which are typical of upwelling relaxation in the area (deCastro et al., 2004). An  
390 exception of strong downwelling-favourable wind from the south was recorded on July  
391 4.

392 Surface flow off the *rias* had a northward direction with a speed ranging between 0.5  
393 and  $7.5 \text{ cm s}^{-1}$  (Fig. 5B). On July 3, SST ranged between 16-17 °C inside the *rias*, but an  
394 area with temperature higher than 17 °C was observed outside the *rias*. In the next SST  
395 image (July 9) an increase in temperature was recorded in the *rias Baixas* and the  
396 adjacent area (Fig. 6). The temperature increase was confirmed by the Seawatch data  
397 (Fig. 5C). The daily mean water temperature off the *rias Baixas* increased from 16.4 °C,  
398 in the first days of July up to 18 °C in a period of 10 days after the upwelling.

399 Two MERIS (FR) images (Fig. 7) from the study area were available during state 1, one  
400 on July 3 and the other on July 9. In both, several high chl $a$  "patches" were mapped  
401 inside and in the outer parts of the *rias*. In the area off the external coast of the *rias* the  
402 chl $a$  concentration in the images remained at levels close to 0 mg m $^{-3}$ . This pattern of  
403 the phytoplankton biomass principally confined in the *rias* while in neighbouring shelf  
404 area the chl $a$  levels remained very low, seems to be generated by the northward flow of  
405 surface waters outside the *ria*. The development of northward currents in the relaxation  
406 following intense north winds, responsible for the upwelling recorded at the end of  
407 June, may introduce water of high chl $a$  to the three *rias* from the ocean area outside  
408 them in the first days of July. The continuing mainly north-westward directed transport  
409 over several days may have been responsible for the chl $a$  distribution observed on July  
410 9, where chl $a$  concentration was significantly higher in the *ria de Arousa* than in the  
411 other two *rias* in the south.

412 Different patterns of the higher chl $a$  areas in the *rias* were mapped during state 1. On  
413 July 3, areas of high chl $a$  concentrations were mapped in the *ria de Arousa* (3-4.5 mg  
414 m $^{-3}$ ) and close to the mouths of the three *rias* (higher than 2 mg m $^{-3}$ ). On July 9, chl $a$   
415 concentrations greater than 2 mg m $^{-3}$  were mapped mainly in the middle and inner parts  
416 of the *ria de Vigo* and in the outer part of the *ria de Arousa*.

417 In the image obtained on July 3, areas of high chl $a$  concentrations were observed in the  
418 outer part of the three *rias*, whereas chl $a$  decreased towards the inner part of the *rias*.  
419 Varela *et al.* (2008) reported that this gradient is common in the *ria de Pontevedra*  
420 during the upwelling period when the meteorological forcing is the main factor  
421 responsible for the circulation of the *ria*.

422 Six days after the first available image, the gradient of *chl a* in the *rias* described above  
423 was observed only in the *ria de Arousa*. On the contrary, *Vigo* and *Pontevedra* were  
424 characterized by a *chl a* gradient where concentration increased toward inshore. In the  
425 *ria de Pontevedra* areas of higher *chl a* were recorded at the innermost part and close to  
426 the northern mouth of the *ria*. In the rest of the *ria de Pontevedra* *chl a* concentration  
427 was close to 0 mg m<sup>-3</sup>. In the inner part of *ria de Vigo*, MERIS *chl a* varied between 2  
428 and 3 mg m<sup>-3</sup>. MERIS data delivered from areas like the most interior, shallow part of  
429 the *rias* normally considered as suspicious because the high abundance of macroalgae  
430 increases the *chl a* signal (Gons et al., 1999) were here characterized as reliable, since  
431 they were confirmed by *in situ* data. Moreover, water transparency in the 20 m station  
432 (St. 1) as determined by the Sechhi disk measurements during the first campaign was 2  
433 meters, decreasing the effect of the bathymetry. This part of the *rias* can be firmly  
434 considered as estuary and during nutrient enrichment from river flows, high  
435 concentrations of *chl a* have been recorded (Evans and Prego, 2003). In this case the  
436 observed relatively high concentrations of *chl a* at the inner part of the two southern *rias*  
437 may be the result of the mixture of estuarine water with Eastern North Atlantic Central  
438 Water (ENACW) combined with high residence times. The different offshore-inshore  
439 gradient of *ria de Arousa* seems to be formed by material transferred to the north from  
440 the *rias de Vigo* and *Arousa* due to the northward surface currents. Differences in  
441 topography and local winds should also be considered as possible factors for the  
442 observed differences. *Ria de Arousa* is considered to be the most productive of the *rias*  
443 *Baixas* (Bode and Varela, 1998). In the classification of Vidal-Romaní (1984) *ria de*  
444 *Arousa* is categorized as open bay, while *ria de Pontevedra* and *ria de Vigo* as fjord-  
445 like. Though fjords have deep quiescent interiors, only intermittently renewed, and a

446 shallow sill at the entrance, while the rias are shallow and have a 2 layer circulation that  
447 reverses between up and downwelling.

448 *State 2 (July 12-21)*

449 State 2 was characterized by 9 d of sustained upwelling favourable winds (Fig. 5A) and  
450 southwest currents of up to  $6 \text{ cm s}^{-1}$  (Fig. 5B). SST maps showed that temperature  
451 ranged between 16-17 °C in the coastal area outside the *rias* (Fig. 6). Temperature  
452 recorded by the Seawatch buoy decreased more than 1 °C during the upwelling (Fig.  
453 5C).

454 The two *chl a* maps (Fig. 7) for this state trace the primary results of the upwelling  
455 favourable winds. On July 16 map areas with the highest *chl a* concentrations were  
456 recorded in the middle part of *ria de Pontevedra*, at the mouth of *ria de Arousa* and  
457 through the entire *ria de Vigo*. The distributions were similar in form in the *ria de Vigo*  
458 and *ria de Pontevedra* but higher *chl a* ( $>2.5 \text{ mg m}^{-3}$ ) was found in the former.  
459 Unpublished data showed the outflow of *ria* water towards offshore in speeds that  
460 reached  $4 \text{ cm s}^{-1}$ . This situation of the surface water being advected offshore in the *rias*,  
461 when upwelling favourable wind started to blowing off the *rias Baixas* is typical of the  
462 positive estuarine circulation that has been described in the area (Fraga and Margalef,  
463 1979; Figueiras and Pazos, 1991). In this two-layer circulation, the offshore surface  
464 Ekman-transport advects the low salinity water out of the *ria*, while the denser upwelled  
465 water flows into the *ria* along the sea bed. The zone of enhanced surface *chl a*  
466 concentration that in the MERIS images extends throughout the *ria de Pontevedra* and  
467 *ria de Vigo* is probably surface water that is flowing out of the *rias* due to the positive  
468 estuarine circulation generated during the upwelling favourable conditions.

469 The July 19 *chl<sub>a</sub>* image shows a noticeable increase in *chl<sub>a</sub>* with concentrations higher  
470 than 1 mg m<sup>-3</sup> over the entire continental shelf zone, although *chl<sub>a</sub>* decreased slightly  
471 within the *rias*. In the study of Ospina-Álvarez et al. (2010) it was found out that during  
472 the upwelling favourable conditions that characterized the Northern Galician *rias* during  
473 the period July 13-22 2008 the ENACW did not enter in the *rias*. While in that period  
474 *chl<sub>a</sub>* in the Northern Galician *rias* did not exceed the value of 1 mg m<sup>-3</sup> (Ospina-Álvarez  
475 et al. 2010), in the *rias Baixas* it was generally higher than 1 mg m<sup>-3</sup>, confirming the  
476 suggestion that there is a difference between Northern and Western (*rias Baixas*)  
477 Galician *rias* with respect to their eutrophication status under the same meteorological  
478 conditions.

#### 479 State 3 (*July 22-31*)

480 As a result of the strong upwelling event a peak of *chl<sub>a</sub>* with concentrations up to 5 mg  
481 m<sup>-3</sup> was mapped on July 22 in the coastal area off Galicia. The high *chl<sub>a</sub>* concentration  
482 was extended from the northern offshore area to the interior of the *rias* (Fig. 7). A  
483 coincident area of relatively low temperature was mapped in the north part of the study  
484 area, whereas an area of warmer water was detected at the south. Differences up to 2 °C  
485 were obtained between the *rias* (Fig. 6). This alongshore difference probably reflects  
486 the persistence of stronger coastal upwelling in the north after the event of 10-21 July  
487 and an earlier onset of relaxation in the south. It is often the case that upwelling is more  
488 persistent in the north of the area (Torres and Barton, 2007). Figure 8 shows the  
489 development of the upwelling on the Galician coast. With the abrupt decrease of  
490 upwelling-favourable to zero wind on July 22, currents at the Seawatch buoy became  
491 briefly northward as expected, but subsequently returned to southward despite the onset  
492 of intermittent northward winds. The last MERIS image (July 29) is consistent with  
493 strong relaxation: the offshore region has near-zero chlorophyll and a region of

494 moderately high chl<sub>a</sub> is bound to the coast. Within the *rias* values tend to be low,  
495 reflecting downwelling conditions. It seems probable that flow more inshore of the  
496 Seawatch buoy was northward and convergent to shore. At the end of July chl<sub>a</sub> in the  
497 *ria de Vigo* showed the lowest concentration of all the images of previous days.

498 The high chl<sub>a</sub> concentrations along the Galician shelf coupled with low SST. MERIS  
499 and MODIS images at the start of this state on July 22 show clearly the presence of a  
500 cold, chlorophyll-rich area resulting from the previous 10 d of upwelling. Although high  
501 chl<sub>a</sub> water was recorded below the surface in the *in situ* profiles (Fig.2B) during the  
502 second sampling in the *ria de Vigo*, MERIS data recorded the low surface values  
503 present. Figueiras and Pazos (1991) noted the presence of nutrient-rich water during a  
504 summer upwelling event in the *rias Baixas* that did not reach the surface, As soon as  
505 upwelling ceases, the 2-layer circulation reverses and surface waters flow inwards and  
506 sink to the lower layer carrying with them the higher surface concentrations of Chl<sub>a</sub>.  
507 The possible non uniformity of the Inherent Optical Properties (IOP) in the water  
508 profiles (Stramska and Stramski, 2005) and the development and validation of the water  
509 constituent algorithms based on water samples from certain depths (e.g. O'Reily et al.,  
510 2000; González Vilas et al., 2011) affirms the necessity of the *in situ* data.

511 Although this high biomass area was not sampled directly, *in situ* data from the *ria de*  
512 *Vigo* revealed relatively high concentrations of diatoms (mainly *Chaetoceros* spp.),  
513 small flagellates (personal observation). The ASP producer *Pseudo-nitzschia* was also  
514 present in the *ria de Vigo* but in relatively low concentrations. This phytoplankton  
515 composition seems to be typical in the *rias Baixas* during the summer according to the  
516 annual cycle of phytoplankton abundance proposed in 1987 by Figueiras and Niel.  
517 Moreover, Frangopulos et al., (in press) mentioned the presence of the red-tide

518 dinoflagellate *Noctiluca scintillans* in high abundances in *ria de Vigo* during summer  
519 2008.

#### 520 **4. Summary and conclusions**

521 Three different states of meteorological and oceanographic periods were identified in  
522 the area during the July of 2008. Surface currents and winds off the *rias Baixas* affected  
523 the distribution of *chl a* in the *rias Baixas*. At the beginning of July (State 1) the variable  
524 and weak wind and the resulting northward surface currents limited the high *chl a*  
525 concentrations to the *rias* so that only low *chl a* values were found in the offshore area.  
526 Differences in the topography of the *rias*, effects of local winds and transport by  
527 currents between the *rias* seem to be the main factors for the observed differences in the  
528 gradients of *chl a* along the *rias* between *ria de Arousa* and the two southern *rias* (*Vigo*,  
529 and *Pontevedra*). MERIS images obtained during State 2 showed the first response of  
530 *chl a* distribution due to the strong favourable winds that were blowing in the area. With  
531 the development of strong upwelling the circulation in the *rias* is reinforced in the  
532 estuarine sense so that *chl a* increases rapidly there. After a period of six days of  
533 continued upwelling, *chl a* concentrations higher than  $1\text{mg m}^{-3}$  were observed in all the  
534 area mapped according to MERIS data. State 3 commences with the appearance of a  
535 high biomass algal event coincident with the area of low SST as the culmination of the  
536 preceding, extended upwelling. The weak northward winds that characterized this state  
537 permitted downwelling that transferred *chl a* rich water toward the *rias*. The upwelled  
538 water was recorded in the *chl a* profiles in the *ria de Vigo* but was missed by the  
539 MERIS. The continuing downwelling circulation resulted in decay of the bloom and  
540 subduction of surface waters in the *rias* compatible with the decrease of *chl a* observed  
541 in the last MERIS image. Although MERIS has a repeat interval of three days, cloud  
542 cover prevented acquisition of all possible images. Nevertheless the 6 images obtained

543 in July 2008 captured the main changes in *chl a* concentration and distribution during the  
544 three periods of different meteorological and oceanographic states.

545 Previous ocean colour studies by satellite sensors (CZCS, SeaWiFS, MODIS) in the  
546 Western Iberian Peninsula (WIB) during an upwelling event (McClain et al., 1986;  
547 Peliz and Fiuza, 1999; Joint et al., 2001; Bode et al., 2003; Ribeiro et al., 2005; Oliveira  
548 et al., 2009a, Oliveira et al., 2009b) played an important role in the identification of *chl a*  
549 patterns and study of harmful algal blooms and primary production but were restricted  
550 to the ocean shelf because of insufficient spatial resolution. Another problem that  
551 affected many of the previous satellite remote sensing application studies in the study  
552 area was the failure of the algorithms used to provide reliable *chl a* data during  
553 upwelling favourable conditions especially in the areas closest to the coast. Upwelling  
554 waters are characterized by considerable variability in the vertical distribution of  
555 phytoplankton (Brown and Hutchings, 1987) and in the optical properties (Morel and  
556 Prieur, 1977). Optically active water constituents such as SPM which are brought into  
557 the surface because of the strong mixing that takes place during upwelling events may  
558 vary independently of the surface *chl a* as in the typically shallow estuarine Case 2  
559 waters. On the other hand, the present study allows more detailed examination of the  
560 *chl a* distribution in the Galician *rias* and the adjacent area during a summer upwelling  
561 cycle due to the finer spatial resolution and precise atmospheric correction offered by  
562 MERIS. The application of an algorithm specially developed for the study area provides  
563 more accurate mapping of *chl a*, which has, for the first time to our knowledge, provided  
564 surface *chl a* mapping of the interior of the *rias Baixas*. Moreover, the fine resolution of  
565 MERIS in combination with the local-based algorithm permitted the detailed detection  
566 of relative high biomass "patches" in the *rias* and the coastal area. There was a  
567 significant variation in the timing and the extent of the *chl a* peak areas. The maps show



568 that the spatial structure of the phytoplankton distribution in the study area can be  
569 complex. Some of these areas of high *chl<sub>a</sub>* that are apparent in satellite images can be  
570 missed by *in situ* monitoring programmes. High *chl<sub>a</sub>* levels in the *rias* due to the  
571 increase in the concentration of harmful phytoplankton species have been recorded in  
572 the past especially in summer (GEOHAB, 2005). An example of a localized feature is  
573 that constantly high surface *chl<sub>a</sub>* was observed in the Bay of Baiona, located in the  
574 southern mouth of *ria de Vigo* in all the images (Figure 9). The Bay of Baiona is  
575 characterized as the zone of *ria de Vigo* where harmful algal events due to species like  
576 *Alexandrium minutum* are a frequent and recurrent phenomenon (Bravo et al., 2010). It  
577 is worth noting that for the area seaward of the *rias* all the algorithms used in this study  
578 came up with very similar values and patterns for *chl<sub>a</sub>*. Moreover, this study showed  
579 that the synergy of two space borne sensors (MERIS, MODIS) in combination with *in*  
580 *situ* data can be of great help in the monitoring, detection and study of high biomass  
581 algal events in an coastal upwelling areas.

## 582 **Acknowledgements**

583 MERIS data were obtained through ESA/ENVISAT project AO-623. We are very  
584 grateful to A. Acuña and D. Perez Estevez for their helpful assistance during the field  
585 work. This work was partially funded by the European Commission's Marie Curie  
586 Actions (project 20501 ECOSystem approach to Sustainable Management of the Marine  
587 Environment and its living Resources [ECOSUMMER]) through a grant supported ES.

## 588 References

589

590 Aiken, J., Moore, G., F., Trees, C., C., Hooker, S., B., & Clark, D., K. (1995). The  
591 SeaWiFS CZCS-type pigment algorithm. In, *SeaWiFS Technical Report Series* (p. 34).  
592 Greenbelt MD.

593 Atkinson, P.M., & Tatnall, A.R.L. (1997). Introduction Neural networks in remote

594 sensing. *International Journal of Remote Sensing*, 18, 699-709.

595 Bezdek, J.C. (1981). *Pattern Recognition with Fuzzy Objective Function Algorithms*.  
596 New York: Plenum.

597 Bode, A., & Varela, M. (1998). Primary production and phytoplankton in three Galician  
598 Rias Altas (NW Spain): seasonal and spatial variability. *Scientia Marina*, 62(4), 319-330.

599 Bravo, I., Figueroa, R.I., Garcés, E., Fraga, S., & Massanet, A. (2010). The intricacies  
600 of dinoflagellate pellicle cysts: The example of *Alexandrium minutum* cysts from a bloom-  
601 recurrent area (Bay of Baiona, NW Spain). *Deep Sea Research Part II: Topical Studies in*  
602 *Oceanography*, 57, 166-174.

603 Brown, C., A., Huot, Y., Werdell, P., J., Gentili, B., & Claustre, H. (2008). The origin  
604 and global distribution of second order variability in satellite ocean color and its applications to  
605 algorithm development. *Remote Sensing of Environment*, 112, 4186-4203.

606 Doerffer, R., & Schiller, H. (2007). The MERIS Case 2 water algorithm. *International*  
607 *Journal of Remote Sensing*, 28, 517-535.

608 Doerffer, R., & Schiller, H. (2008). MERIS Regional Coastal and Lake Case 2 Water  
609 Project - Atmospheric Correction ATBD. In: GKSS Research Center 21502 Geestacht.

610 Dzwonkowski, B., & Yan, X., -H. (2005). Development and application of a neural  
611 network based ocean colour algorithm in coastal waters. *International Journal of Remote*  
612 *Sensing*, 26, 1175-1200.

613 EC (2000). Directive of the European Parliament and of the Council 2000/60/EC  
614 establishing a framework for community action in the field of water policy. *Official Journal of*  
615 *the European Communities*, L327/321.

616 Evans, R., H., & Gordon, H., R. (1994). Coastal zone color scanner system calibration:  
617 A retrospective examination. *Journal of Geophysical Research*, 99, 7293-7307.

618 Evans, G., & Prego, R. (2003). Rias, estuaries and incised valleys: is a ria an estuary?  
619 *Marine Geology*, 196, 171-175.

620 Figueiras, F., & Pazos, Y. (1991). Microplankton assemblages in three Rías Baixas  
621 (Vigo, Arosa and Muros, Spain) with a subsurface chlorophyll maximum: their relationships to  
622 hydrography. *Marine Ecology Progress Series*, 76, 219-233.

623 Figueiras, F.G., & Ríos, A.F. (1993). Phytoplankton succession, red tides and the  
624 hydrographic regime in the Rías Bajas of Galicia. In T.J. Smayda & Y. Shimizu (Eds.), *Toxic*  
625 *Blooms in the Sea* (pp. 239-244). New York: Elsevier.

626 Figueiras, F.G., Jones, K.J., Mosquera, A.M., Alvarez-Salgado, X.A., Edwards, E., &  
627 MacDougall, N. (1994). Red tide assemblage formation in an estuarine upwelling ecosystem:  
628 Ria de Vigo. *Journal of Plankton Research*, 16, 857-878.

629 Fraga, F. (1981). Upwelling off the Galician coast North West Spain. In E. Suess. & J.  
630 Thiede (Eds.), *Coastal upwelling* (pp. 176-182). New York: Plenum Publishing Corp.

631 Fraga, S., Anderson, D.M., Bravo, I., Reguera, B., Steidinger, K.A., & Yentsch, C.M.  
632 (1988). Influence of upwelling relaxation on dinoflagellates and shelfish toxicity in Ria de Vigo,  
633 Spain. *Estuarine Coastal Shelf Science*, 27, 349-361.

634 Garder, K., L., Chen, F., R., Lee, Z., P., Hawes, S., K., & Kamykowski, D. (1999).  
635 Semianalytic moderate-resolution imaging spectrometer algorithm for chlorophyll a  
636 concentration and absorption with bio-optical domains based on nitrate-depletion temperatures.  
637 *Journal of Geophysical Research*, 104, 5403-5421.

638 Garder, K., L., & Steward, R., G. (1985). A remote-sensing reflectance model of a red-  
639 tide dinoflagellate off west Florida. *Limnology and Oceanography*, 30, 286-298.

640 GEOHAB (2005). Global Ecology and oceanography of Harmful Algal Blooms  
641 (GEOHAB). In G. Pitcher, T. Moita, V. Trainer, R. Kudela, F.G. Figueiras & T. Probyn (Eds.),  
642 *GEOHAB Core Research Project: HABs in Upwelling Systems* (p. 82 p.). Paris and Baltimore:  
643 IOC and SCOR.

644 Gigueiras, F.G., & Niell, F.X. (1987). Composición del fitoplankton de la ría de  
645 Pontevedra (NO de España). *Investigación Pesquera*, 51, 371-409.

646 Gitelson, A., A., Schalles, J., F., & Hladik, C., M. (2007). Remote chlorophyll-a  
647 retrieval in turbid, productive estuaries: Chesapeake Bay case study. *Remote Sensing of*  
648 *Environment*, 109, 464-472.

649 González Vilas, L., Spyrakos, E., & Torres Palenzuela, J., M. (2011). Neural network  
650 estimation of chlorophyll a from MERIS full resolution data for the coastal waters of Galician  
651 rias (NW Spain). *Remote Sensing of Environment*, 115, 524-535.

652 Gons, H. (1999). Optical Teledetection of Chlorophyll a in turbid inland waters.  
653 *Environmental Science & Technology*, 33, 1127-1132.

654 Gons, H.J., Auer, M.T., & Effler, S.W. (2008). MERIS satellite chlorophyll mapping of  
655 oligotrophic and eutrophic waters in the Laurentian Great Lakes. *Remote Sensing of*  
656 *Environment*, 112, 4098-4106.

657 Hornik, K., Stinchcombe, M., & White, H. (1989). Multilayer feed-forward networks are  
658 universal approximators. *Neural Networks*, 2, 359-366.

659 Jeffery, S., Mantoura, R., & Wright, S. (1997). *Phytoplankton pigments in*  
660 *oceanography: guidelines to modern methods*. Paris, France: UNESCO Publishing.

661 Keiner, L., E., & Yan, X., H. (1998). A neural network model for estimating sea surface  
662 chlorophyll and sediments from thematic mapper imagery. *Remote Sensing of the Environment*,  
663 66, 153-165.

664 Kratzer, S., Brockmann, C., & Moore, G. (2008). Using MERIS full resolution data to  
665 monitor coastal waters - A case study from Himmerfjärden, a fjord-like bay in the northwestern  
666 Baltic Sea. *Remote Sensing of Environment*, 112, 2284-2300.

667 Margalef, R. (1956). Estructura y dinámica de la "purga de mar" en Ría de Vigo.

668 *Investigacion Pesquera*, 5, 113-134.

669 McClain, C., R., Feldman, G., C., & Hooker, S., B. (2004). An overview of the  
670 SeaWiFS project and strategies for producing a climate research quality global ocean bio-optical  
671 time series. *Deep-Sea Research II*, 51, 6-42.

672 Morel, A., Claustre, H., Antoine, D., & Gentili, B. (2007). Natural variability of bio-  
673 optical properties in Case 1 waters: Attenuation and reflectance within the visible and near-UV  
674 spectral domains as observed in South Pacific and Mediterranean waters. *Biogeosciences*, 4,  
675 2147-2178.

676 Morel, A., & Prieur, L. (1977). Analysis of variations in ocean color. *Limnology and*  
677 *Oceanography*, 22, 709-722.

678 Muller-Karger, F., E., McClain, C., R., Sambrotto, R., N., & Ray, G., C. (1990). A  
679 comparison of ship and coastal zone color scanner mapped distribution of phytoplankton in the  
680 southeastern Bering Sea. *Journal of Geophysical Research*, 95, 483-499.

681 Nogueira, E., Perez, F.F., & F., R.A. (1997). Seasonal patterns and long-term trends in  
682 an estuarine upwelling ecosystem (Ria de Vigo, NW Spain). *Estuarine Coastal and Shelf*  
683 *Science*, 44, 185-300.

684 Odermatt, D., Giardino, C., & Heege, T. (2010). Chlorophyll retrieval with MERIS  
685 Case-2-Regional in perialpine lakes. *Remote Sensing of Environment*, 114, 607-617.

686 O'Reily, J., E., Maritorena, S., Siegel, D., A., O'Brien, M., C., Toole, D., & Mitchell, B.,  
687 G. et al (2000). Ocean color chlorophyll a algorithms for SeaWiFS, OC2 and OC4. In (p. 49):  
688 NASA Technical Memorandum 2000-206892.

689 Robinson, I. (2004). *Measuring the Oceans from Space: The principles and methods of*  
690 *satellite oceanography*. Chichester, UK: Springer.

691 Shahraiyni, H., T., Shouraki, S., B., Fell, F., Schaale, M., Fischer, J., Tavakoli, A.,  
692 Preusker, R., Tajrishy, M., Vatandoust, M., & Khodaparast, H. (2009). Application of an active  
693 learning method to the retrieval of pigment from spectral remote sensing reflectance data.  
694 *International Journal of Remote Sensing*, 30, 1045-1065.

695 Tillstone, M., B. M., Figueiras, F.G., & Fermín, E.G. (2003). Phytoplankton  
696 composition, photosynthesis and primary production during different hydrographic conditions at  
697 the Northwest Iberian upwelling system. *Marine Ecology Progress Series*, 252, 89-104.

698 Tilstone, G.H., Figueiras, F.G., & Fraga, F. (1994). Upwelling-downwelling sequences  
699 in the generation of red tides in a coastal upwelling system. *Marine Ecology Progress Series*,  
700 112, 241-253.

701 Torres, R., & Barton, E.D. (2007). Onset of the Iberian upwelling along the Galician  
702 coast. *Continental Shelf Research*, 27, 1759-1778.

703 Varela, M. (1992). Upwelling and phytoplankton ecology in Galician (NW Spain) rías  
704 and shelf waters. *Boletín del Instituto Español de Oceanografía*, 8, 57-74.

705 Vidal-Romaní, J. R. (1984). A orixe das rias galegas: Estado da censtión (1886-1983).  
706 Cuardenos da Área de Ciencias Mariñas, Seminario de Estudos Galegos. Vol. 1. Edición do  
707 Castro. A Coruña, Spain.

708 Zhang, T., Fell, F., Liu, Z., -S., Preusker, R., Fischer, J., & He, M., -X. (2003).  
709 Evaluating the performance of artificial neural network techniques for pigment retrieval from  
710 ocean color in Case I waters. *Journal of Geophysical Research*, 108, 3286-3298.

711

712

713

714

715

716

717

718

719

720

721

722

723

724

725

726 **Tables and graphs**

727 Table 1. MERIS imagery showing the acquisition time (UTC) and mean view zenith  
 728 angle from west. Sea-truthing ranges of chlorophyll *a* (chl*a*), suspended particulate  
 729 matter (SPM), percentage of inorganic contribution to SPM and Secchi disk depth (Zsd)  
 730 for *ria de Vigo* (12 stations) during the two samplings.

Chl <i>a</i> (mg m <sup>-3</sup> )		0.03-2.65		0.03-2.72		
SPM (mg L <sup>-1</sup> )		1.45-2.48		1.17-3.15		
inorganic matter (%)		36-56		38-58		
Zsd (m)		2-12		2.5-7		
MERIS FR	July 03 2008	July 09 2008	July 16 2008	July 19 2008	July 22 2008	July 29 2008
Acquisition time (UTC)	10:59	11:10	10:50	10:56	11:02	10:42
View zenith angle (°)	13.5	13.0	20.7	15.3	11.7	20.7

731

732 Table 2. Percentage of pixels belonging to each cluster over the study area (*rias Baixas*),  
 733 obtained from classification images derived from the MERIS images used in this study.

734

Date	<i>ria</i>	Cluster#1	Cluster#2	Cluster#3
July 03 2008	Vigo	74.22	23.95	1.83
	Pontevedra	62.50	37.35	0.15
	Arousa	76.33	22.55	1.13
July 09 2008	Vigo	95.40	4.04	0.55
	Pontevedra	96.14	3.57	0.30
	Arousa	94.24	3.01	2.75
July 16 2008	Vigo	84.52	15.48	0.00
	Pontevedra	70.48	28.78	0.73
	Arousa	49.56	47.19	3.25
July 19 2008	Vigo	82.17	17.66	0.17
	Pontevedra	83.68	16.18	0.15
	Arousa	75.68	22.48	1.84
July 22 2008	Vigo	87.41	11.88	0.71
	Pontevedra	90.06	9.79	0.15
	Arousa	82.92	15.86	1.22
July 29 2008	Vigo	72.43	27.57	0.00
	Pontevedra	24.17	75.40	0.43
	Arousa	11.67	86.60	1.73

735

736

737

738 Table 3. Performance parameters for the Chl*a* neural networks tested in this study

Chla model	Data base	R <sup>2</sup>	RMS error (mg m <sup>-3</sup> )	Relative RMS error %
NNRB#1 MERIS C2R Processor	Whole	0.17 0.09	0.74 0.80	93 90
NNRB#2 MERIS C2R Processor	Cluster#1	0.24 0.09	0.69 0.80	85 90
NNRB#3 MERIS C2R Processor	Cluster#1 High quality	0.70 0.04	0.46 0.90	65 89

739

740

741 Table 4. Dominant atmospheric and oceanographic conditions off the *rias Baixas*  
742 categorized as three different states during the upwelling cycle in summer 2008.

Period	Date	Dominant atmospheric and oceanographic conditions off <i>rias Baixas</i>
1	July 1-10	winds blowing mainly in south direction ( $I_w = -108$ ) after a period of favourable upwelling winds, mostly northward surface flow
2	July 11-21	strong north winds ( $I_w = 900$ ), surface flow towards southwest
3	July 22-31	mainly south blowing winds ( $I_w = -230$ ), southward surface flow

743

744

745

746

747

748

749

750

751

752

753 Fig. 1. A) Galician coast and bathymetry of the area. From north to south the *rias*  
754 *Baixas: Muros y Noya, Arousa, Pontevedra* and *Vigo*. The location of the Seawatch  
755 buoy station off Cabo Silleiro is shown by a black rectangle. B) Map of *ria de Vigo*  
756 showing the locations of the sampling stations. The MERIS FR pixel size is presented in  
757 relation to the size of the *ria*.

758 Fig. 2. Plots of chlorophyll *a* fluorescence ( $\text{mg m}^{-3}$ ) vertical profiles for the upper 10 m  
759 of the water column in *ria de Vigo* on A) July 09 2008 and B) July 22 2008. Also I  
760 would put the date actually in each panel for clarity.

761

762 Fig. 3. Regression analysis between Total Suspended Material (TSM, also termed  
763 Suspended Particulate Matter) and *chl a* concentrations. ( $y=1.76+0.13x$ ,  $R^2=0.1$  and  
764 sample size  $N=41$ ).

765

766 Fig. 4. Classification of MERIS images derived from the study area. The 3 classes  
767 identified using the FCM are shown.

768

769 Fig. 5. A) Daily upwelling index off the *rias Baixas*. The  $I_w$  in  $\text{m}^{-3} \text{s}^{-1} 100\text{m}^{-1}$  represents  
770 the offshore Ekman flux in the surface layer. Arrows indicating the days where MERIS  
771 FR images were available and numbers the different states identified during the studied  
772 period and cycles the days of sampling. B) Surface currents ( $\text{cm s}^{-1}$ ) recorded by the  
773 Seawatch buoy station located off Cape Silleiro ( $42^\circ 7.8'N$ ,  $9^\circ 23.4'W$ ). Data were daily  
774 averaged from 0 a.m. on July 1 2008 to 12 p.m. on July 31 2008. Symbols as in Fig. 2.



775 C) Daily average of sea temperature for the month of July 2008 off the *rias Baixas*. All  
776 data are means  $\pm$  1 S.D.

777

778 Fig. 6. MODIS-derived Sea Surface Temperature maps for *rias Baixas* and adjusted  
779 coastal waters during the upwelling cycle of July 2008. White patches represent clouds.

780

781 Fig. 7. Chl $a$  maps for MERIS FR data derived during the upwelling cycle of July 2008  
782 in the study area. Land and clouds were masked and they appear with white colour.

783

784 Fig. 8. RGB MERIS (12) FR composite image acquired on July 22 2008 over the study  
785 area. Land was masked with black colour.

786

787

788

789

790

791

792

793

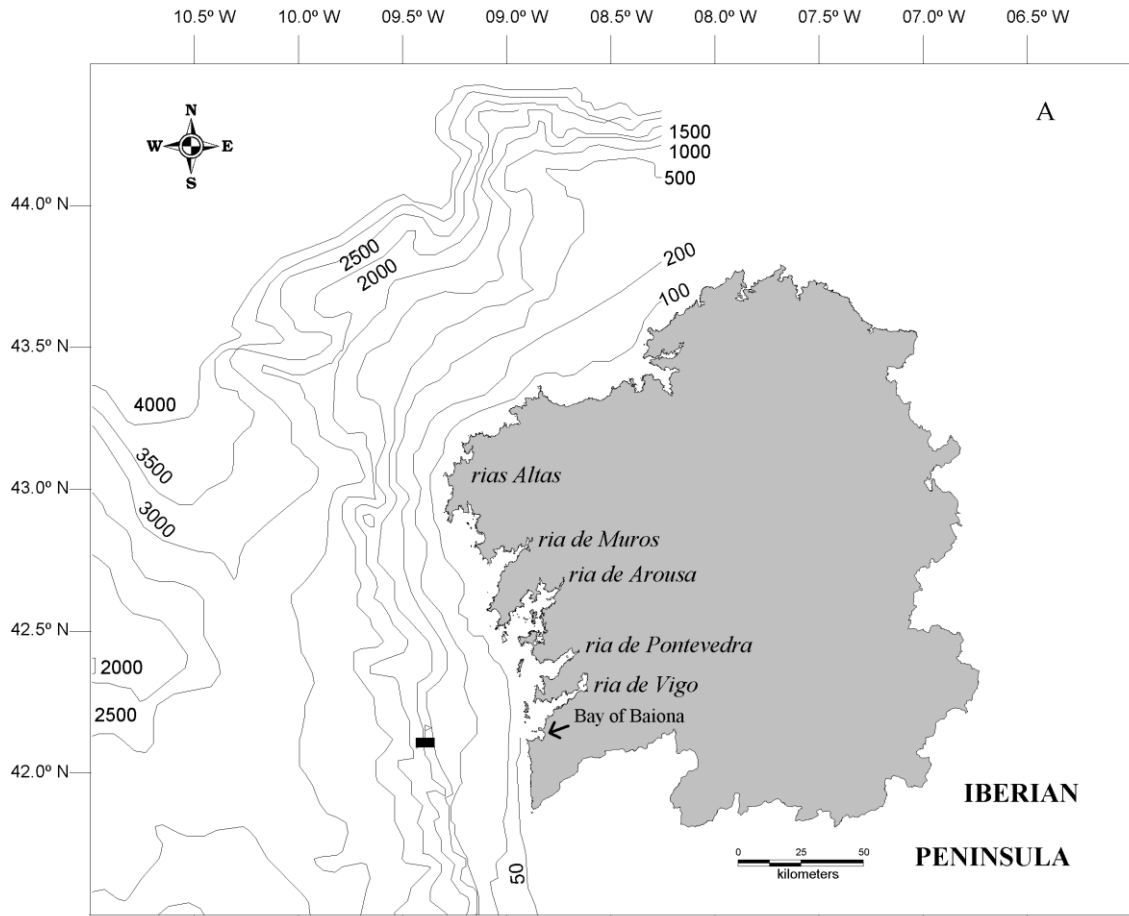
794

795

796

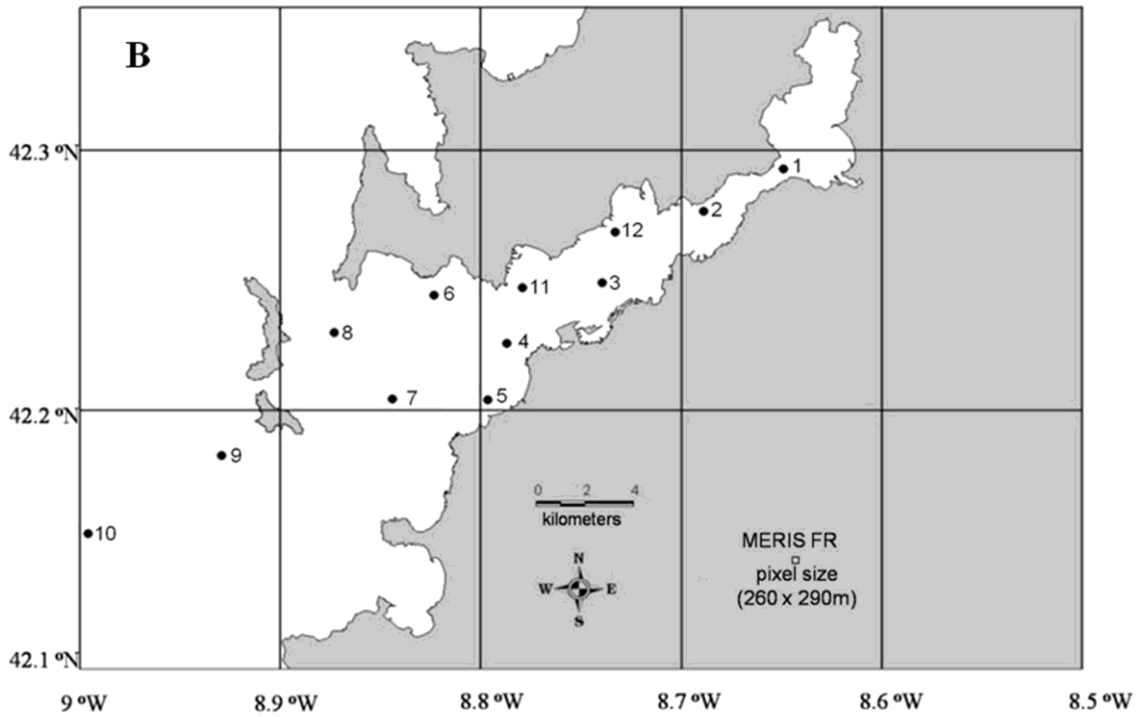
797

798

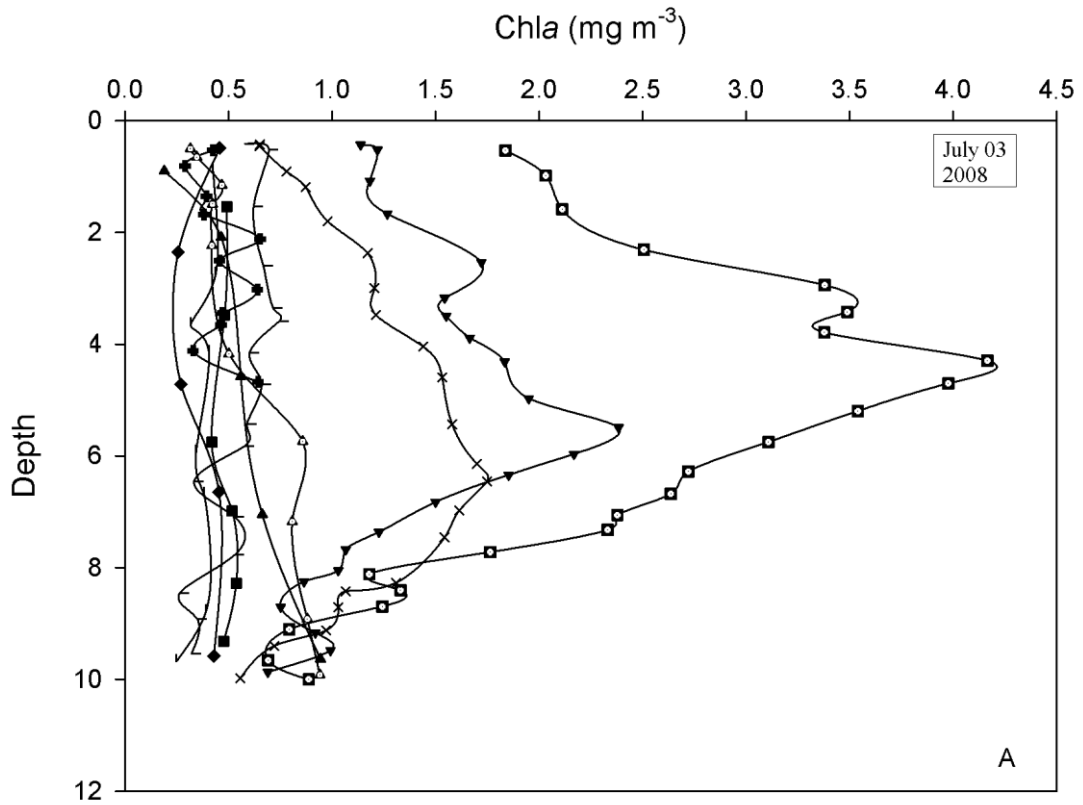


799

800

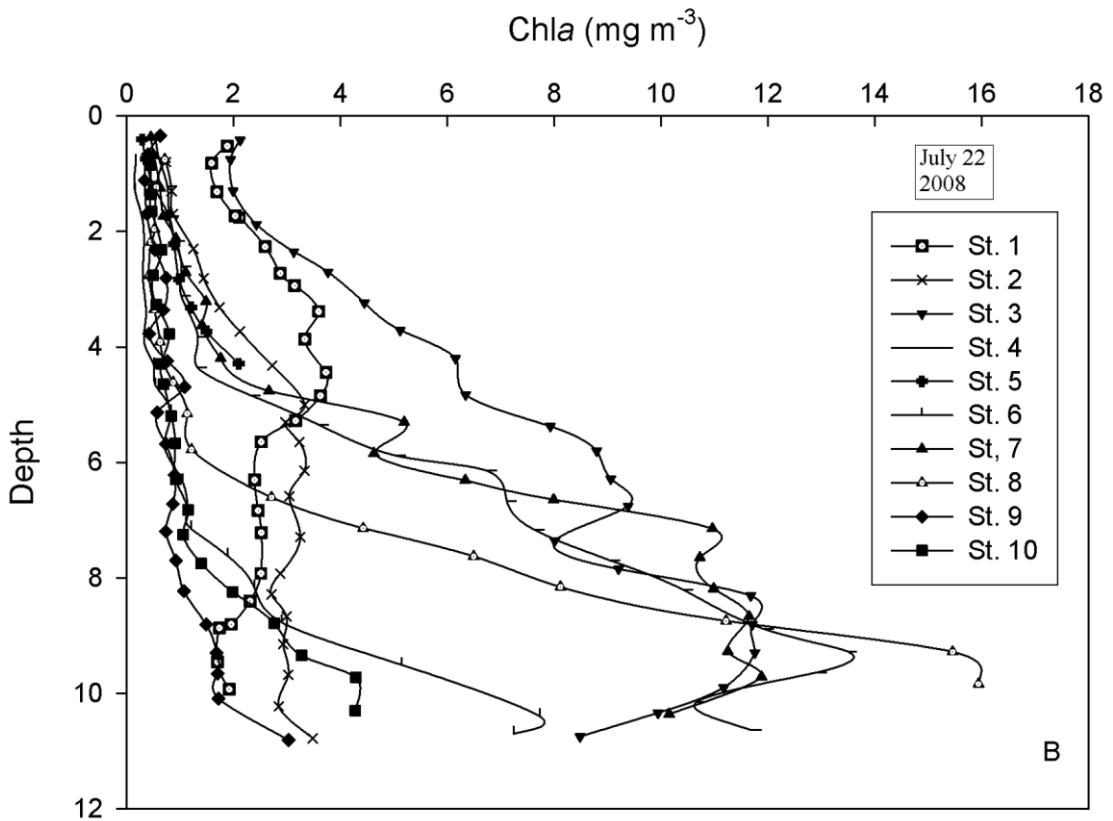


801

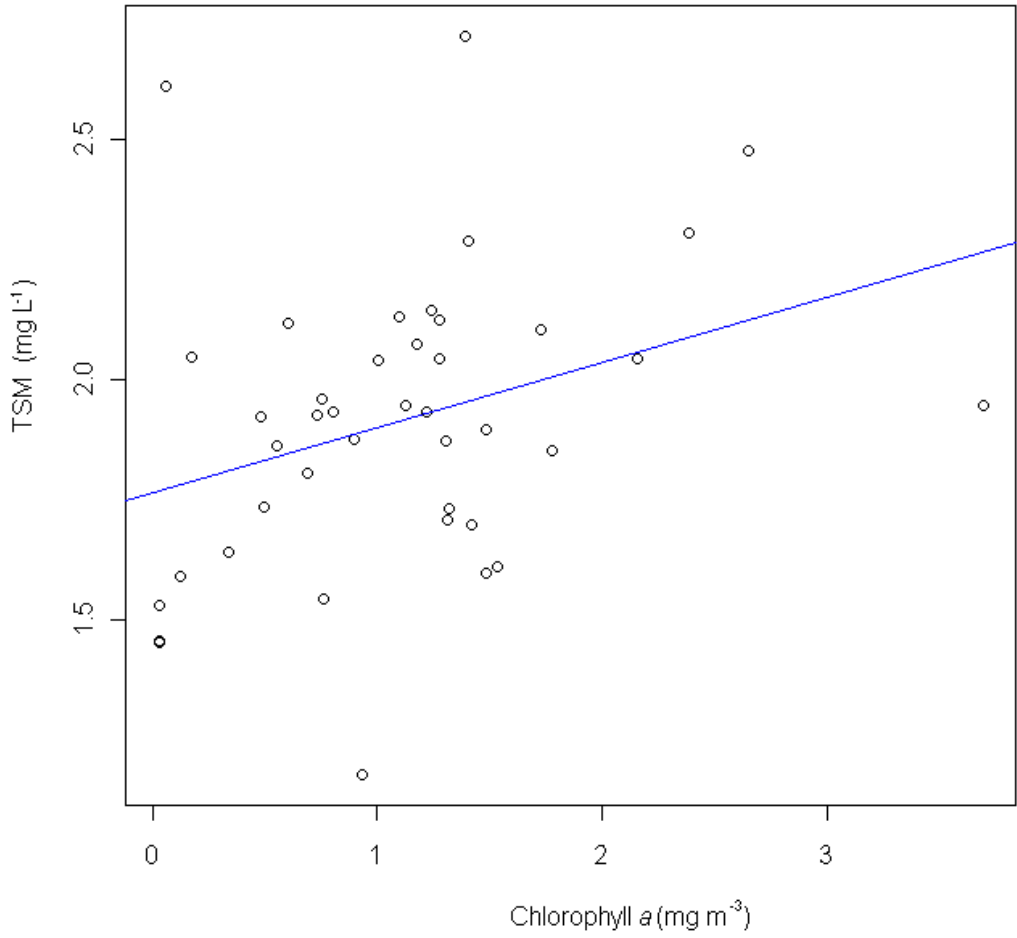


802

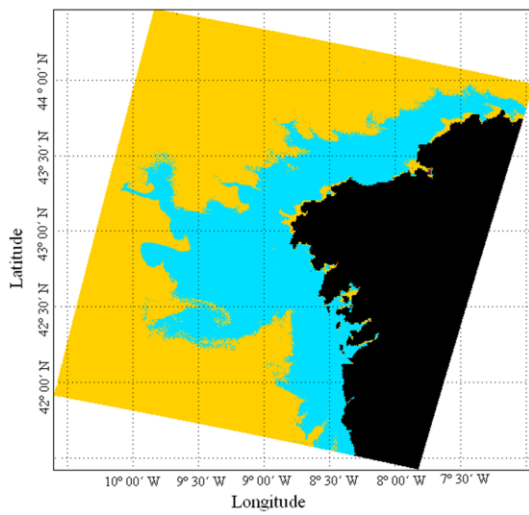
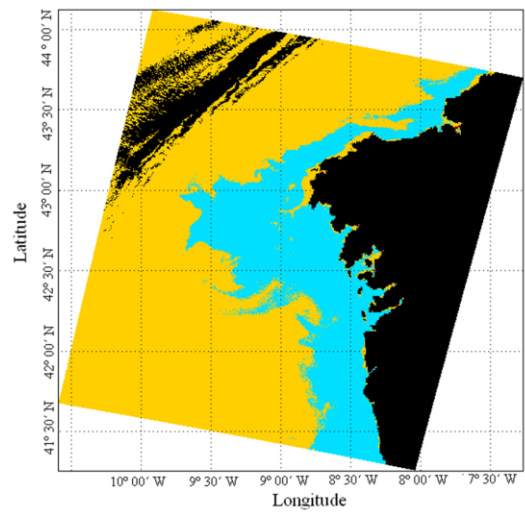
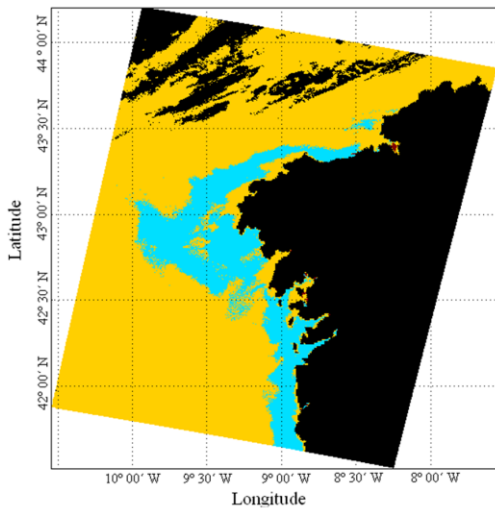
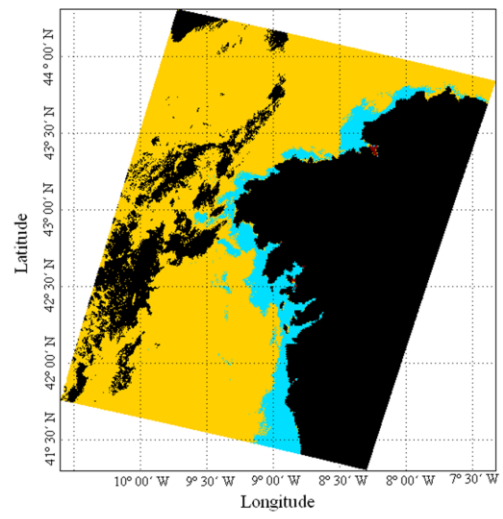
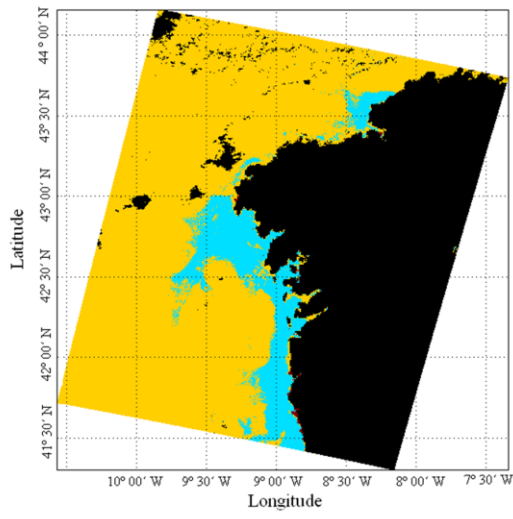
803



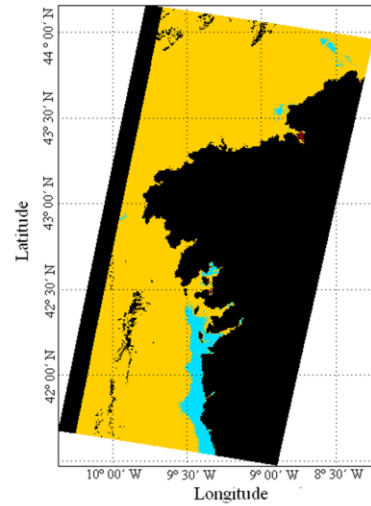
804



805

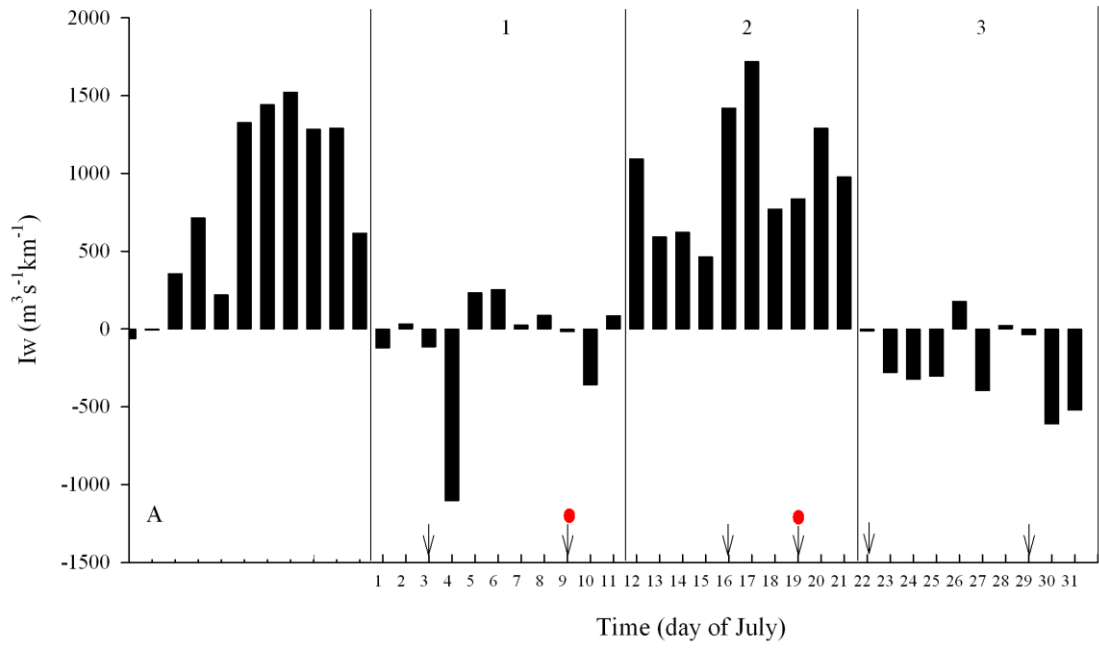


- Cluster#1
- Cluster#2
- Cluster#3



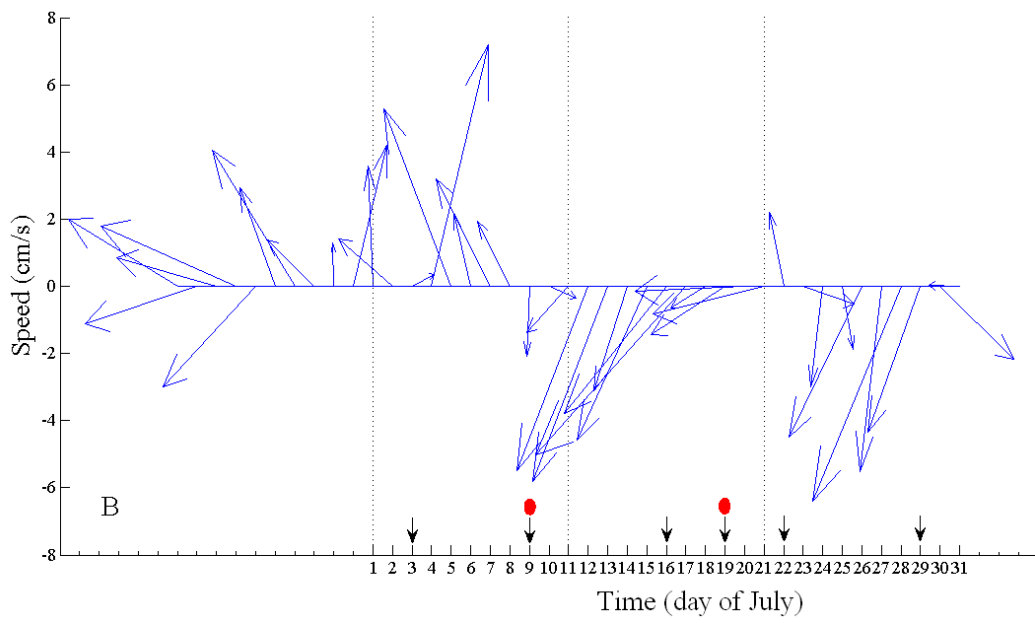
806

807



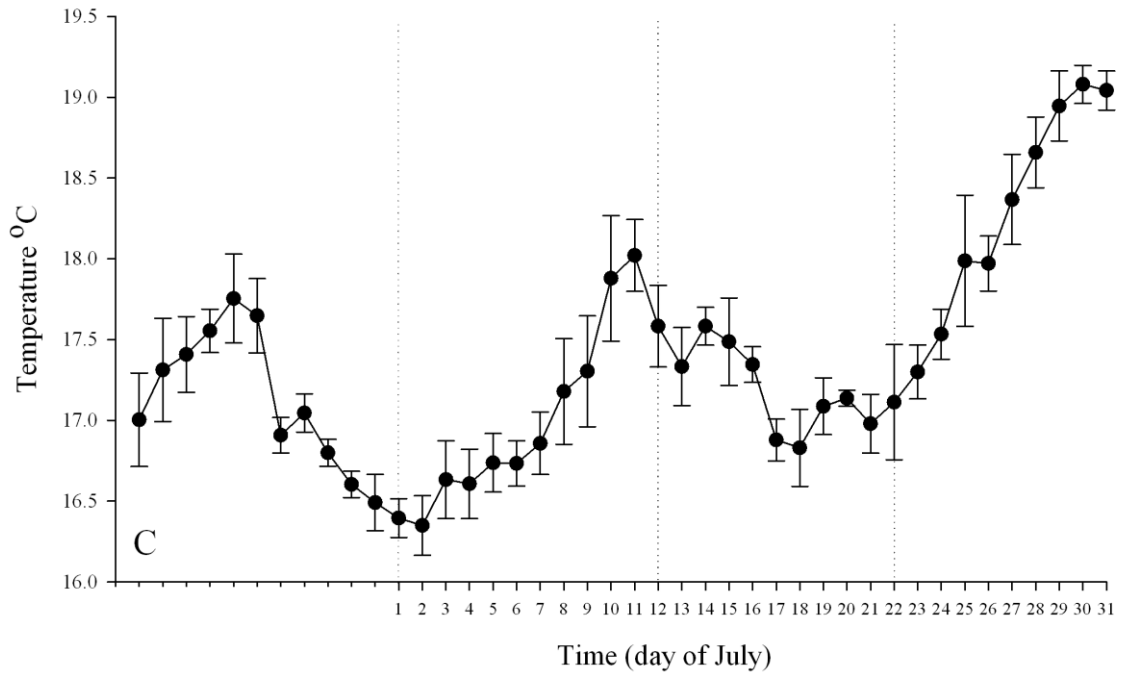
808

809



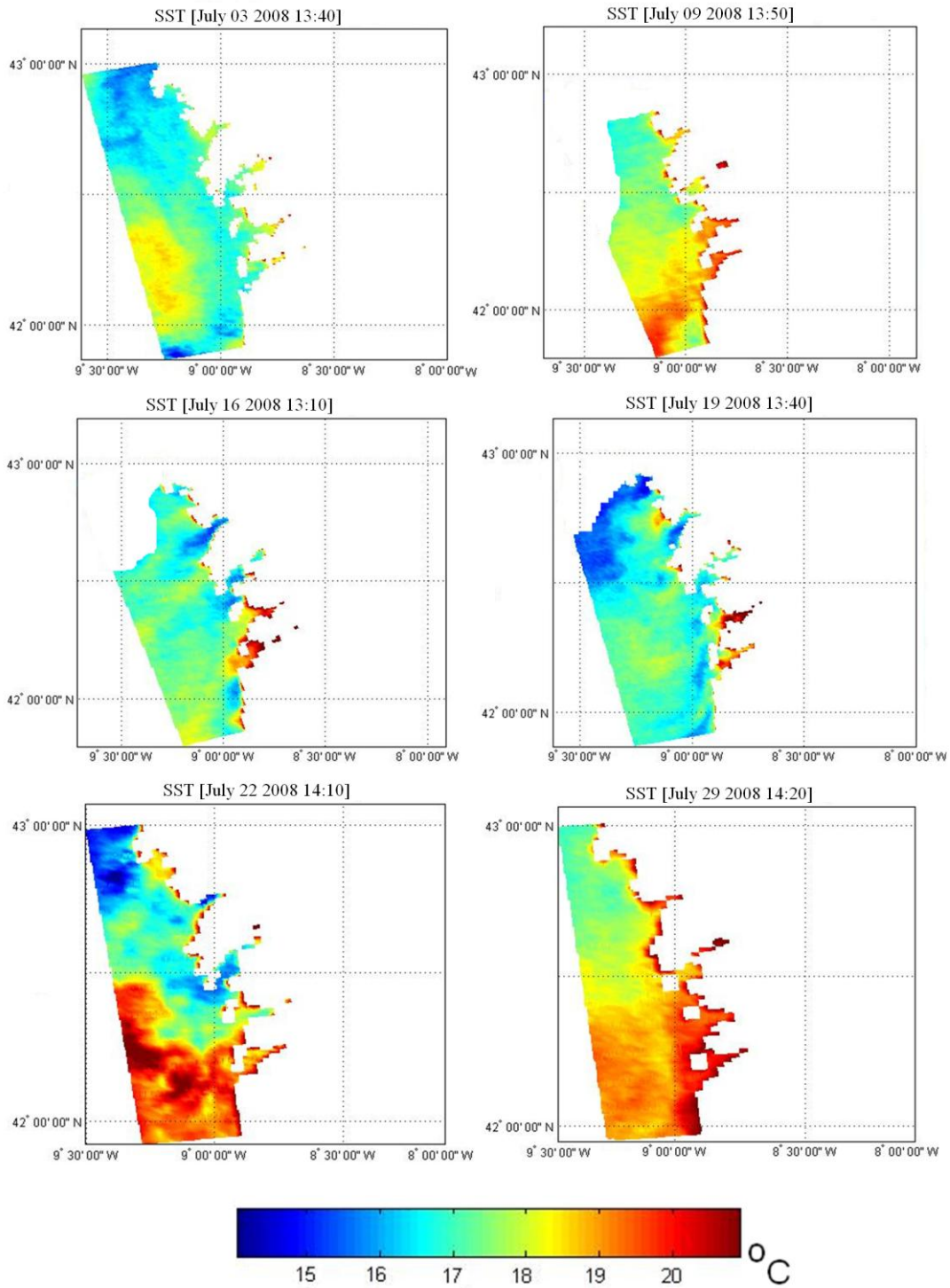
810

811



812

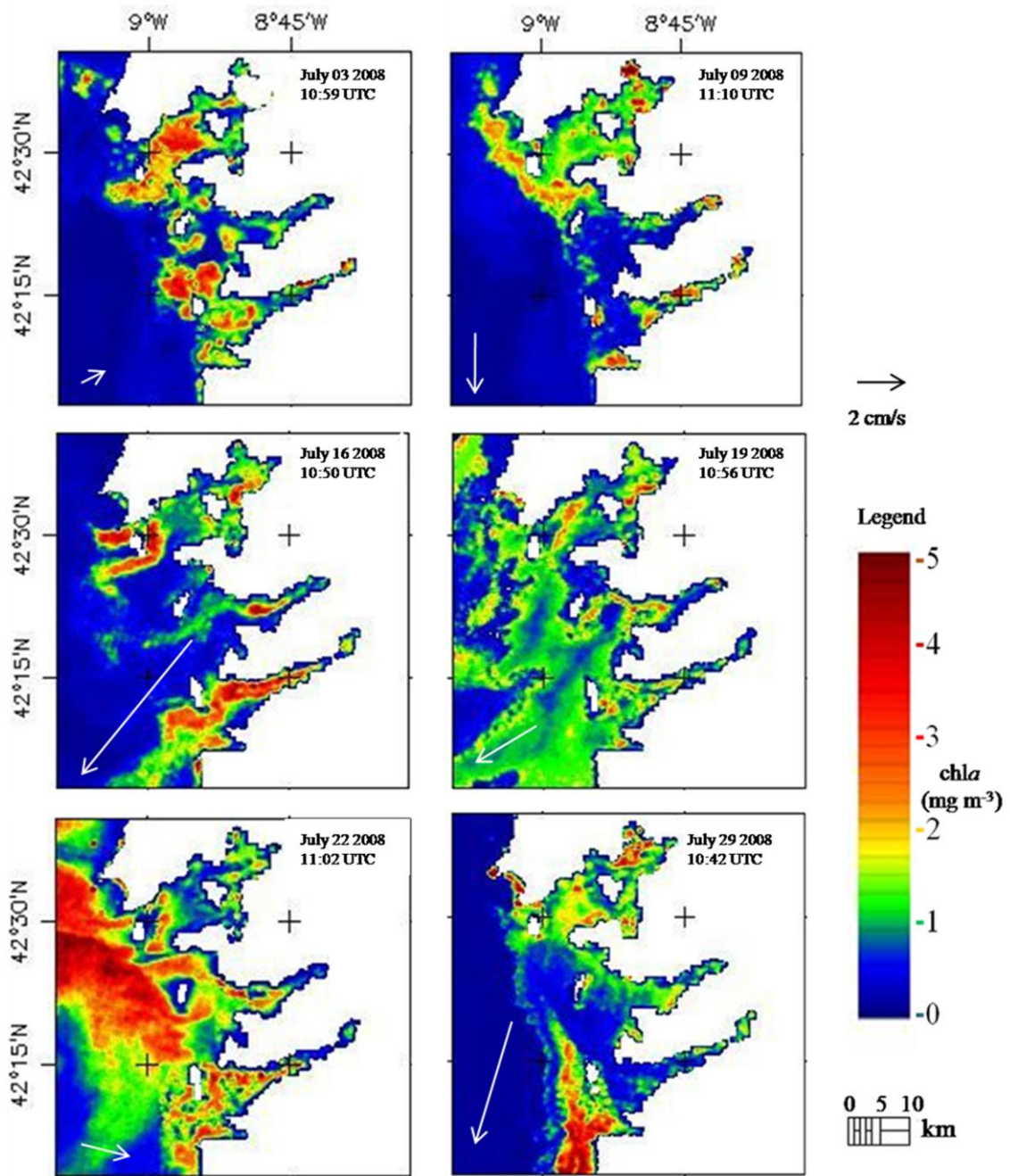
813



814

815

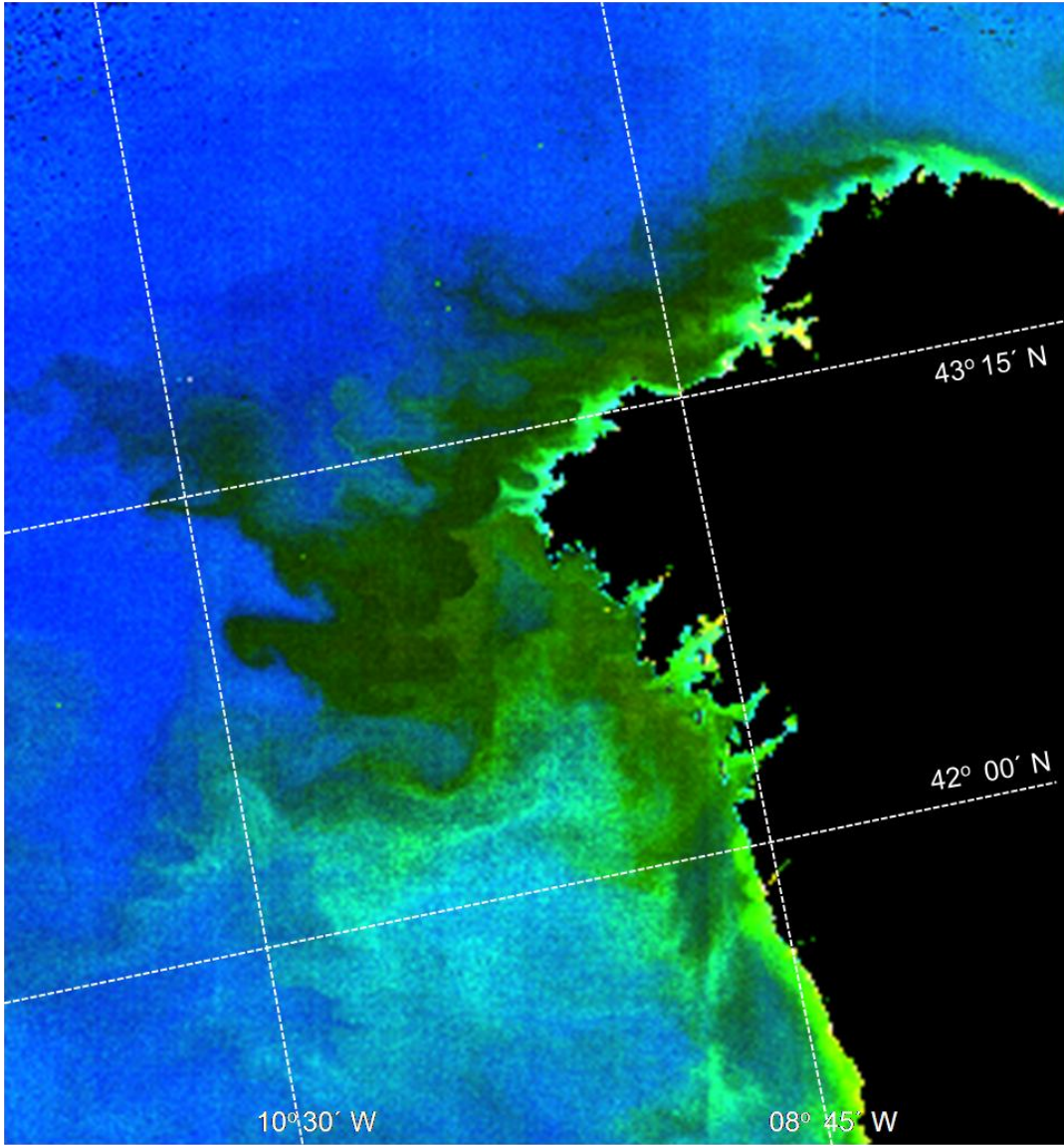




816

817

818



819